Title

Analysis of the Amyloidogenic Potential of Pufferfish (Takifugu rubripes) Islet Amyloid Polypeptide Highlights the Limitations of Thioflavin-T Assays and the Difficulties in Defining Amyloidogenicity

Journal

Biochemistry, 55(3)

ISSN

0006-2960

Authors

Wong, Amy G
Wu, Chun
Hannaberry, Eleni
et al.

Publication Date

2016-01-26

DOI

10.1021/acs.biochem.5b01107

Peer reviewed

HHS Public Access

Author manuscript

Biochemistry. Author manuscript; available in PMC 2017 July 10.

Published in final edited form as:

Biochemistry. 2016 January 26; 55(3): 510–518. doi:10.1021/acs.biochem.5b01107.

Analysis of the Amyloidogenic Potential of Pufferfish (*Takifugu rubripes*) Islet Amyloid Polypeptide Highlights the Limitations of Thioflavin-T Assays and the Difficulties in Defining Amyloidogenicity

Amy G. Wong[1], **Chun Wu**[2], **Eleni Hannaberry**[1], **Matthew D. Watson**[1], **Joan-Emma Shea**[2], and **Daniel P. Raleigh**[1,*]

[1]Department of Chemistry, Stony Brook University, Stony Brook, NY 11794-3400

[2]Department of Chemistry and Biochemistry, University of California at Santa Barbara, Santa Barbara, CA 93106-9510

Abstract

Islet amyloid polypeptide (IAPP, amylin) forms pancreatic amyloid in type-2 diabetes, a process that contributes to the loss of β-cell mass in the disease. IAPP has been found in all higher organisms examined, but not all species form amyloid and the ability to do so correlates with the primary sequence. The amyloidogenic potential of fish IAPPs have not been examined, although fish have been proposed as a source for xenobiotic transplantation. The sequence of pufferfish IAPP (*Takifugu rubripes*) is known and is the most divergent from human IAPP of any reported IAPP sequence, differing at eleven positions including seven located within residues 20 to 29, a segment of the molecule that is important for controlling amyloidogenicity. Several of the substitutions found in pufferfish IAPP are non-conservative including Ser to Pro, Asn to Thr, Ala to Tyr and Leu to Tyr replacements and several of these have not been reported in mammalian IAPP sequences. Amyloid prediction programs give conflicting results for pufferfish IAPP. CD spectroscopy, FTIR, and transmission electron microscopy reveal that pufferfish IAPP forms amyloid and does so more rapidly than human IAPP in tris buffer at pH 7.4, but does so more slowly in phosphate buffered saline (PBS) at pH 7.4. Molecular dynamics simulations indicate that the pufferfish sequence is compatible with models of IAPP amyloid. The fish polypeptide does not significantly bind to thioflavin-T in tris and does so only weakly in PBS. The results highlight difficulties with thioflavin-T assays and the ambiguity in defining amyloidogenicity.

Keywords

Diabetes; Amylin; Islet Amyloid Polypeptide; Amyloid; Thioflavin-T; Islet Transplantation

*Author to whom correspondence should be addressed: daniel.raleigh@stonybrook.edu, Phone: (631) 632-9547, Fax: (631) 632-7960.

Supporting Information

Supporting Information Available: A table of predicted amyloidogenicity of p-IAPP relative to h-IAPP. A figure showing the RMSD of the models of human and pufferfish IAPP from the starting structures during the time course of a 500 ns MD simulation. A figure showing the final snapshots of the structures at the end of each simulation.

Amyloid formation and aberrant protein aggregation play important roles in a diverse range of disorders including Alzheimer's disease, Parkinson's disease, and type-2 diabetes. The neuropancreatic polypeptide hormone human islet amyloid polypeptide (h-IAPP, also known as amylin) forms islet amyloid in the pancreas in type-2 diabetes.[1–3] The process of islet amyloid formation contributes to β-cell dysfunction in the disease and to the failure of islet transplants.[1–9] Mature IAPP is a 37 residue polypeptide which has been found in all higher organisms examined and is highly conserved, but not all species form amyloid and the ability to do so correlates with the primary sequence of IAPP. Teleostean fish have been proposed as a source for xenobiotic transplantation and for studies of diabetes mellitus, in part because in teleostean fish the pancreatic exocrine tissue is separated from the pancreatic endocrine cells, facilitating the isolation of the endocrine cells.[10–15] However, the amyloidogenicity of fish IAPP amyloidogenicity is not well understood and this is an issue for islet transplantation.[8, 9] The amyloidogenic potential of any full-length fish IAPP has not been examined, although a ten residue fragment of salmon IAPP has been studied experimentally and larger fragments derived from different fish have been analyzed computationally.[11, 12] The complete sequence of pufferfish IAPP (*Takifugu rubripes*) is known and diverges the most from human IAPP of any reported IAPP sequence, differing at eleven positions, including multiple substitutions in regions believed to be important for amyloid formation (Figures-1, 2).

Here we examine the ability of pufferfish IAPP (p-IAPP) to form amyloid *in vitro*. The analysis reveals that the relative amyloidogenicity, as defined by the kinetics of amyloid formation, of human and pufferfish IAPP depend on solution conditions and thus amyloidogencity is context dependent. The analysis also highlights complications with the widely applied thioflavin-T assay of amyloid formation and provides more evidence that they can lead to false negatives.

Amyloid formation *in vitro* is commonly followed using fluorescence detected thioflavin-T binding assays.[16, 17] Thioflavin-T is a small dye whose quantum yield increases and whose emission maximum shifts upon binding to amyloid fibrils.[18] There are no high resolution structures of thioflavin-T bound to amyloid fibrils, but the dye is believed to bind to the surface of the cross-β structure of the amyloid fibrils.[17–21] The parallel, in register β-sheet structures of typical amyloid fibrils create a series of grooves that run parallel to the long axis of the fibril and these are believed to form the thioflavin-T binding sites. Binding of the dye fixes the position of the dimethylaminobenzyl and benzothiazole rings of thioflavin-T and reduces self-quenching, thereby leading to the enhancement in quantum yield. Thioflavin-T assays are the most widely applied biophysical technique used to follow amyloid formation. They are simple, easy to apply and have proven to be very informative, but the dye provides an extrinsic probe of amyloid formation and the signal depends on the amount of dye bound and the quantum yield of the bound dye.[17, 18] Thus, the relationship between the intensity of thioflavin-T fluorescence and the amount of amyloid formed is not always clear and it is formally possible that the assay could give false positives and false negatives.[22]

Materials and Methods

Peptide Synthesis and Purification

Peptides were synthesized with a CEM microwave peptide synthesizer on a 0.10 mmol scale utilizing 9-fluorenylmethoxycarbonyl (Fmoc) chemistry. 5-(4'-Fmoc-aminomethyl-3',5-dimethoxyphenol) valeric acid (PAL-PEG) resin was used to provide an amidated C-terminus. Fmoc-protected pseudoproline (oxazolidine) dipeptide derivatives were utilized as previously described.[23, 24] Solvents used were ACS-grade. β-branched residues, the first residue attached to the resin, pseudoproline dipeptide derivatives and the residues following the pseudoproline dipeptide derivatives were double-coupled. Peptides were cleaved from the resin via standard trifluoroacetic acid (TFA) methods. The cleaved crude peptides were dissolved into 15% (v/v) acetic acid and lyophilized. The disulfide bond was formed in 100% dimethyl sulfoxide at room temperature. Peptides were purified via reverse-phase high-performance liquid chromatography (RP-HPLC) using a Higgins Analytical Proto 300 C18 preparative column (10 mm × 250 mm). The purity of the peptides was tested using analytical HPLC. The masses of the pure peptides were confirmed with MALDI time-of-flight mass spectrometry. h-IAPP, expected 3903.6, observed 3902.9; p-IAPP, expected 3948.9, observed 3949.4.

Sample Preparation and Fluorescence Assays

Stock solutions were prepared by dissolving peptide into 100% hexafluoroisopropanol (HFIP) at 1.6 mM. Solutions were filtered with 0.45 μM Acrodisc syringe filters and the required amount was lyophilized overnight to remove HFIP. Dry peptide was then dissolved into tris buffer or PBS for the fluorescence assays. The kinetics of amyloid formation were monitored using thioflavin-T binding assays conducted at 25 °C. Fluorescence measurements were performed using a Beckman Coulter DTX 880 plate reader with a multimode detector using an excitation wavelength of 430 nm and an emission wavelength of 485 nm.

Transmission Electron Microscopy (TEM)

TEM images were collected at the Life Science Microscopy Center at the State University of New York at Stony Brook. At the end of each experiment, 15 μL aliquots of the samples used for the kinetic studies were removed, blotted on a carbon-coated 300-mesh copper grid for 1 min and then negatively stained with saturated uranyl acetate for 1 min.

Circular Dichroism

Far UV CD experiments were performed on an Applied Photophysics Chirascan CD spectrophotometer. The sample was incubated on the bench for two weeks and the spectrum was recorded. The spectrum was an average of three repeats recorded over a range of 190 – 260 nm, at 1 nm intervals. A 10 mm quartz cuvette was used and a background spectrum was subtracted from the collected data. Experiments were performed at 25 °C in 20 mM tris buffer at pH 7.4. The sample concentration was 40 μM.

FTIR Spectroscopy

FTIR spectra were recorded on a Bruker Vertex 80 FTIR spectrometer equipped with a globar source, KBr beamsplitter and a liquid nitrogen-cooled mercury cadmium telluride (MCT) detector. Spectra were recorded as the result of 2048 scans at a resolution of 1 cm^{-1} using a Bruker BioATR II cell. The effective path length of the cell was approximately 6–8 μm. Experiments were performed at 20 °C and a protein concentration of 600 μM.

Molecular Dynamics Simulations and Modeling of Pufferfish and Human Amyloid Fibrils

The two initial fibril structures of human IAPP (two layers of 5 peptides) were taken from two sources: one derived from solid state NMR studies of full length human IAPP and the other from crystal structures of small “steric zipper” peptides derived from the human IAPP sequence. The two initial fibril structures of pufferfish IAPP were derived from the two experimental fibril structures of human IAPP by mutating the corresponding residues (Figure-1A). Each of the four initial fibril structures was immersed in a truncated octahedral box ($a = b = c$ = ~69 Å, $\alpha = \beta = \gamma = 109.47°$) filled with water molecules. The all-atom point-charge force field (AMBER ff03)[25] was used to represent the peptides. This force field has been successfully used to model the binding of Aβ(39–42) to Aβ40/ Aβ42 peptides[26], the binding among Aβ protofibrils[27] and the binding of fluorescent dyes to Aβ protofibrils.[28] The water solvent was explicitly represented by the TIP3P model.[29] The AMBER 14 simulation suite[30] was used in molecular dynamics simulations and data analysis. After an initial energy minimization, a total of 4 simulations (one run for each fibril system) were performed with different initial random velocities. The random velocities of atoms were generated according to the Maxwell-Boltzmann distribution at 300 K. The production run (500 ns) was performed at 300 K and was comprised of 1 ns of molecular dynamics in the NPT ensemble mode (constant pressure and temperature) to equilibrate the solvent and 499 ns dynamics in the NVT ensemble mode (constant volume and temperature). Periodic boundary conditions were imposed on the system. The particle-mesh Ewald method[31] was used to treat the long-range electrostatic interactions. SHAKE[32] was applied to constrain all bonds connecting hydrogen atoms, enabling a 2 fs time step used in the dynamics. To reduce computation time, non-bonded forces were calculated using a two-stage RESPA approach[33] where the short-range forces within a 10 Å radius were updated every step and the long range forces beyond 10 Å are updated every two steps. Langevin dynamics were used to control the temperature (300 K) using a collision frequency of 1 ps^{-1}. The center of mass translation and rotation was removed every 500 steps to remove the “block of ice” problem.[34, 35] The trajectories were saved at 50 ps intervals for analysis.

Results

The primary sequence of h-IAPP and p-IAPP are compared in Figure-1A, the location of the residues in p-IAPP that differ from those in h-IAPP is also displayed within the context of a structural model of the h-IAPP amyloid fibril (Figure-1B).[36] The structured core of the h-IAPP amyloid fibril is thought to be comprised of residues 8 to 37.[36–38] All eleven of the changes in p-IAPP relative to h-IAPP are found within this 30 residue segment. Of the eleven differences in the sequence, seven are found between residues 22 and 29, a segment which has been proposed to be important for modulating amyloidogenicity.[39–42] p-IAPP

also contains a His-18 to Arg substitution. This replacement is known to reduce the amyloidogenicity of h-IAPP and modulates IAPP toxicity in cell culture.[43, 44] The pufferfish polypeptide also includes an Asn-14 to Asp substitution relative to h-IAPP which has been reported in other fish IAPPs, but not in mammals. Other substitutions which have not been reported in mammals include a Leu-27 to Tyr replacement and the replacement of Phe-23 by Ile (Figure-2).

Amyloid Prediction Algorithms Give Conflicting Results for the Relative Amyloidogenicity of Pufferfish IAPP

A range of amyloid prediction programs have been developed and most rely on physicochemical analysis of the properties of the primary sequence, although the ZipperDB algorithm uses a template approach based on steric zippers.[45–50] The different methods lead to different predictions for the relative amyloidogenicity of h-IAPP and p-IAPP (Supporting Table-1). AGGRESCAN and AmylPred predict h-IAPP is more amyloidogenic than p-IAPP, while TANGO and ZipperDB predict that it is less amyloidogenic and Zyggregator and PASTA predict that there is no change. Thus, existing methods to predict amyloidogenicity give ambiguous results when applied to p-IAPP. Amyloid prediction algorithms have also been shown to improperly predict the amyloidogenicity of scrambled peptide sequences derived from the N-terminal segment of the Huntingtin peptide.[51] The ability of any full-length fish IAPP to form amyloid has not yet been experimentally evaluated.

Pufferfish IAPP Forms Amyloid, But Does not Bind to Thioflavin-T in Tris Buffer

We compared the time course of amyloid formation by human and pufferfish IAPP using thioflavin-T fluorescence assays and by transmission electron microscopy (TEM). We conducted initial experiments in 20 mM tris at pH 7.4, chosen because this buffer has been used extensively in studies of amyloid formation by IAPP. The concentration of IAPP used was 16 μM, again chosen because it is typical of values used for biophysical studies with the polypeptide. A 2-fold excess of thioflavin-T was used. Most experiments with h-IAPP avoid a large excess of thioflavin-T to avoid any perturbation of the kinetics of amyloid formation. Thioflavin-T does not impact the kinetics of IAPP aggregation under these conditions.[52] A sigmoidal thioflavin-T fluorescence time course, consisting of a lag period, a growth phase and final plateau is observed in the presence of h-IAPP which is characteristic of amyloid formation (Figure-3A). No change in thioflavin-T intensity is observed for the sample of p-IAPP, even for a time which is 6-fold longer than the lag time of human IAPP amyloid formation (Figure-3A). The standard interpretation of these results would be that pufferfish IAPP is not amyloidogenic under these conditions. However, time-dependent TEM studies show that this is not the case (Figure-3B). Aliquots were collected at five different time points, including two time points within the lag phase of h-IAPP amyloid formation. Samples were removed at t= 0, $0.25t_{50}$, $2t_{50}$, $3t_{50}$ and $5t_{50}$, where t_{50} refers to the time required for human IAPP to reach half maximum fluorescence intesnsity in a thioflavin-T assay. As expected, no amyloid fibrils are detected in the samples of h-IAPP removed at t = 0, and t = $0.25t_{50}$, In contrast, amyloid fibrils are clearly present in the p-IAPP sample at the $0.25t_{50}$ time point (Figure-3B). Mats of amyloid fibrils are observed for both h-IAPP and p-IAPP in samples removed at 24 hours and at subsequent time points even though no change in thioflavin-T fluorescence intensity is detected for the p-IAPP sample. These experiments

clearly indicate that thioflavin-T based assays give a misleading view of p-IAPP amyloid formation. The thioflavin-T assays displayed in Figure-3A involved monitoring the fluorescence intensity at 485 nm. We confirmed that the lack of a change in the signal of the p-IAPP sample is not a consequence of the emission wavelength chosen by collecting complete fluorescence emission spectra of thioflavin-T in the absence of peptide and in the presence of either human or pufferfish IAPP amyloid fibrils. The spectra of thioflavin-T alone or in the presence of p-IAPP amyloid are essentially identical with a weak emission maximum near 520 nm (Figure-4). In contrast, the emission maximum is shifted to near 480 nm in the presence of h-IAPP amyloid fibrils and there is a significant enhancement in quantum yield. The lack of thioflavin-T signal could be due to changes in the surface structure of the amyloid fibrils that lead to weaker dye binding, or be caused by changes in the quantum yield of the bound dye. A lower yield of fibrils will also lead to a weaker thioflavin-T signal. Another potential factor that can lead to lower thioflavin-T is changes in the association of fibrils. If the fibrils tightly associate, the dye binding surfacing could potentially be occluded, leading to fewer thioflavin-T binding sites.

The TEM images of h-IAPP and p-IAPP amyloid fibrils are very similar (Figure-3B), but it is difficult to detect molecular level changes in structure by TEM, given the resolution of the method and the negative stains employed. Thus, we turned to circular dichroism (CD) to probe the secondary structure of the p-IAPP fibrils. A sample of p-IAPP was prepared and incubated until amyloid fibrils were formed, as judged by TEM, and the CD spectrum recorded (Figure-5A). The CD spectrum of the pufferfish peptide exhibits a broad minimum near 218 nm, consistent with β-sheet structure, and the shape of the spectrum is very similar to that reported for the h-IAPP amyloid fibrils.

We also recorded the Fourier-transform infrared (FTIR) spectra of h-IAPP and p-IAPP (Figure-5B). The amide-I mode is sensitive to secondary structure, exhibiting characteristic shifts to lower energy, lower wavenumber, observed in β-sheets. There is considerable variability in the FTIR spectra of amyloid, but most amyloids exhibit a broad peak near the region of 1615 to 1630 cm^{-1} while random coil features are found at higher wavenumbers.[53] Monomeric h-IAPP has been reported to give an FTIR spectrum with a broad peak centered near 1645 to 1650 cm^{-1}. [54] Our experimental spectrum of h-IAPP exhibits a peak at 1627 cm^{-1} while p-IAPP displays a peak at 1635 cm^{-1}. In both cases, the peak is shifted away from the random coil position. The relatively modest difference in band position for the two polypeptides suggests that there could be differences in the structure of the aggregates. MD simulations, described in a subsequent section, provide a possible explanation for the difference.

The Relative Rates of Amyloid Formation by Human and Pufferfish IAPP are Dependent on the Choice of Buffer

We next examined the behavior of h-IAPP and p-IAPP in a more physiological buffer consisting of 20 mM sodium phosphate, 140 mM KCl at pH 7.4 (PBS). A typical thioflavin-T curve is observed for h-IAPP in PBS with a shorter lag phase than observed in tris (Figure-6). The shorter lag phase is consistent with the known effects of salts on IAPP amyloid formation.[55] A weak thioflavin-T signal is observed from the p-IAPP sample under

these conditions, but the final thioflavin-T intensity is 15 to 20-fold weaker than observed for the h-IAPP sample. Somewhat surprisingly, the time required to reach the plateau of the thioflavin-T response is longer for the p-IAPP sample in PBS relative to the time required for h-IAPP to form amyloid even though p-IAPP forms amyloid more rapidly in tris buffer. A TEM time course confirms this observation. Amyloid fibrils are detected from the sample of h-IAPP before they are observed in the p-IAPP sample. Thus, the relative rate of amyloid formation by p-IAPP and h-IAPP depends upon the choice of buffer, an observation which indicates discussions of relative amyloidogenicity should be treated with caution.

Pufferfish IAPP is Compatible with Existing Models of Human IAPP Amyloid Fibrils

We next performed molecular dynamics simulations to test if the pufferfish sequence is compatible with existing models of the h-IAPP amyloid fibrils. There are two high resolution models of the h-IAPP fibrils: one derived from solid state NMR studies of full length h-IAPP and the other from crystal structures of small “steric zipper” peptides derived from the h-IAPP sequence.[36, 37] While the two models differ in their details, they have many common features and their similarities outweigh their differences. In both structures, the fibril core is made up of two C2 symmetric stacks of monomers (Figure 1B). Each monomer adopts a U-shaped structure which includes two β-strands connected by a less structured linker. The N-terminal strand is on the exterior of the fibril and the C-terminal strand forms the interface between two peptide molecules in one layer. We threaded the pufferfish sequence onto each model structure, here using two stacks of five monomers as the model, and conducted all-atom molecular dynamics simulations of both with explicit solvent model, as detailed in the Methods section. We also ran MD simulations of each model using the human peptide as a control. The 500 ns simulations indicate that the p-IAPP sequence is compatible with the proposed fibril models for h-IAPP, retaining the overall strand-loop-strand fold. The Cα-RMSD at the end of the simulations are shown in Supporting Figure-S1 and the last snapshots of the four simulations are shown in Supporting Figure-S2. The NMR-derived fibril model fits the p-IAPP sequence particularly well, with less than a 1 Å deviation in Cα-RMSD between the h-IAPP and the p-IAPP forms, suggesting that the backbone fold is very similar between human and pufferfish. However, as can be seen from the two representative structures shown in Figure-7, while the overall U-shape fold (β-strand-loop-β-strand) is maintained in p-IAPP, the region adjacent to the loop has more coil and less β-sheet structure than in the case of h-IAPP. This is an interesting observation in light of the FTIR results. The loop which connects the two β-strands also appears to be more flexible in p-IAPP. A notable feature is that the sidechains on the surface of the pufferfish fibrils are more disordered relative to the models of h-IAPP. Our early computational studies of the binding of thioflavin-T to a number of amyloid fibril models showed that the primary binding sites for thioflavin-T were regular grooves formed by ordered side-chains on the surface of amyloid fibrils, with minor sites located the ends of the fibril.[19–21] The lack of ordered grooves on the surface of the p-IAPP fibrils may explain the weak thioflavin-T fluorescence signal, despite clear evidence of fibril formation from TEM.

Thioflavin-T Assays Do Not Accurately Report on Pufferfish IAPP Amyloid Formation Even If the Dye is in Excess

We also examined the effect of increasing the concentration of thioflavin-T to a 20-fold excess relative to IAPP in monomer units. Normally, these concentrations are avoided for fear that high dye concentrations might perturb the kinetics of amyloid formation. The dye has a small impact on the kinetics of h-IAPP amyloid formation, leading to a slightly more rapid time course (Figure-8). A weak thioflavin-T signal is detected when 20-fold excess of dye is added to pufferfish IAPP in tris buffer, but the signal is still weaker than observed for the sample of h-IAPP with a 10-fold lower concentration of dye. The small thioflavin-T signal for the pufferfish IAPP sample exhibits a time course with a longer apparent lag phase (Figure-8A) than h-IAPP. The normal interpretation would be that pufferfish IAPP forms amyloid more slowly than h-IAPP, but generates less amyloid fibers than h-IAPP. However, TEM reveals that this is not the case. Images recorded of samples removed during the lag phase of h-IAPP amyloid formation revealed no detectable fibrils in the h-IAPP samples, but mats of amyloid fibrils were evident in the pufferfish IAPP samples (Figure-8B). This clearly indicates that pufferfish IAPP forms amyloid more rapidly than does h-IAPP under these conditions and provides further evidence that thioflavin-T assays can give misleading results.

Discussion

The data presented here demonstrates that p-IAPP is capable of forming amyloid, but shows that the relative rate of amyloid formation as compared to human IAPP depends upon the choice of buffer. This observation has clear implications for studies which attempt to define and compare the relative amyloidogenicity of different polypeptides. In the present case, the differential effects may reflect the different charge distributions of the two polypeptides. Analysis of the effects of anions on h-IAPP amyloid formation have shown that their effects follow the ion selectivity series at low to moderate concentrations, arguing for a contribution from ion binding.[55] p-IAPP has a lower net charge than h-IAPP due to the Asn to Asp substitution and this may reduce the affinity for phosphate. In this scenario, phosphate accelerates h-IAPP amyloid formation to a greater extent than it does amyloid formation by p-IAPP and this leads to a reversal in the relative rates of amyloid formation. Irrespective of the mechanistic details, the results indicate that solution conditions are important in evaluating relative amyloidogenicity. Our observation that different amyloid prediction programs give differing results for p-IAPP and h-IAPP, together with the context dependent effects described above, and earlier studies on the reliability of amyloidogenicity algorithms indicates that caution should be applied when interpreting the results of amyloidogenicity algorithms.[51]

We believe that the observation of weak or non-existent thioflavin-T binding by p-IAPP is also important. Thioflavin-T is the most widely used probe of amyloid formation and the present study provides a clear cautionary example of the assay yielding a false negative. Thioflavin-T is believed to bind to surface grooves found on amyloid fibrils that are a consequence of their cross-β structure. The large number of substitutions in p-IAPP, 11 out of the 30 residues which are believed to form the core of the fibril, could change the

structure and physicochemical nature of the surface grooves. Our all atom MD simulations show that the pufferfish sequence is compatible with the solid state NMR model of the h-IAPP amyloid fibrils as well as with the model derived from crystal structures of small peptide fragments of h-IAPP. However, two significant differences are observed. First, the part of the region located adjacent to the loop in the U-shape motif adopts coil-like conformations rather than the extended β-sheet conformations seen in h-IAPP. Importantly, the sidechains of the pufferfish IAPP model are more disordered than in the case of the human fibrils and, as a result, do not form the well-ordered surface grooves on the face of the fibril that serve as binding sites for thioflavin-T. The differences in the FTIR spectra of human and pufferfish IAPP are consistent with some structural changes. These differences may contribute to the reduced binding of thioflavin-T to pufferfish IAPP. A reduced yield of amyloid fibrils by the pufferfish peptide could potentially contribute to the lower thioflavin-T signal. In this scenario, p-IAPP forms fewer fibrils and there would be a significant fraction of the polypeptide that remain unaggregated. This seems unlikely, especially given that the CD spectrum and FTIR spectrum indicate that the conformational ensemble is dominated by β-structure. Gravimetric data could formally rule out this possibility but is not available. Again, the mechanistic details of the reduced thioflavin-T signal are not completely clear, but the key result is that thioflavin-T assays can give rise to false negatives and the final thioflavin-T intensity should not be interpreted as a quantitative measure of the amount of amyloid formed when comparing different peptides. Work on Aβ polymorphs and poly-Q peptides as well as a comparison of Aβ(1–40) and Aβ(1–42) also highlights the dangers of quantitative interpretation of thioflavin-T intensities.[56–58]

Finally, we note that teleostean fish have been proposed to be a source of xenobiotic islet transplants. Encouraging success has been obtained using porcine islets for xenobiotic islet transplants, but porcine IAPP is much less amyloidogenic than h-IAPP under all conditions tested and its reduced amyloidogencity correlates with enhanced islet survival.[9] The comparable amyloidogenicity of pufferfish and human IAPP indicates that caution should be used if fish are employed for transplant studies.[12, 14, 15] However, it is also worth noting that the partial sequence of Atlantic wolffish (*Anarhichas lupus*) includes additional proline substitutions as well as additional charge substitutions which likely render the sequence less amyloidogenic and it may be a more attractive candidate for xenobiotic studies.[12] Of course, other factors also need to be addressed when considering candidates for xenobiotic studies. These include the activity relative to human IAPP and immunogenicity. Nonetheless, it will be interesting to examine the behavior of the full-length wolfish sequence once it becomes available (Figure-2).

Supplementary Material

Refer to Web version on PubMed Central for supplementary material.

Acknowledgments

We thank Dr. Robert Tycko for kindly supplying the coordinates of the solid-state NMR based models of the h-IAPP amyloid fibril.

Funding

This work was supported by grants from the United States National Institutes of Health, GM078114, to D.P.R. and from the National Science Foundation (NSF) Grant MCB-1158577 to J.E.S. We acknowledge support from the Center for Scientific Computing at the California Nanosystems Institute (NSF Grant CNS-0960316) and the Extreme Science and Engineering Discovery Environment (XSEDE), supported by National Science Foundation Grant OCI-1053575. We would also like to acknowledge the computational capabilities of the Texas Advanced Computing Center at the University of Texas at Austin (Grants TG-MCA05S027), which provided HPC resources that contributed to the research results reported within this paper (www.tacc.utexas.edu).

Abbreviations

CD	circular dichroism
Cα-RMSD	root mean square deviations of the Cα atomic coordinates
Fmoc	9-fluorenylmethoxycarbonyl
FTIR	Fourier-transform infrared spectroscopy
HFIP	hexafluoroisopropanol
h-IAPP	human IAPP
IAPP	islet amyloid polypeptide or amylin
MALDI	matrix assisted laser desorption/ionization
MD	molecular dynamics
PAL-PEG	5-(4’-Fmoc-aminomethyl-3’,5-dimethoxyphenol) valeric acid
PBS	sodium phosphate saline buffer
p-IAPP	pufferfish IAPP
t_{50}	time required for a human IAPP to reach half maximum fluorescence
TEM	transmission electron microscopy
TFA	trifluoroacetic acid;

References

1. Westermark P, Wernstedt C, Wilander E, Hayden DW, O’Brien TD, Johnson KH. Amyloid Fibrils in Human Insulinoma and Islets of Langerhans of the Diabetic Cat Are Derived from a Neuropeptide-Like Protein Also Present in Normal Islet Cells. PNAS. 1987; 84:3881–3885. [PubMed: 3035556]
2. Cooper GJS, Willis AC, Clark A, Turner RC, Sim RB, Reid KBM. Purification and Characterization of a Peptide from Amyloid-Rich Pancreases of Type 2 Diabetic Patients. PNAS. 1987; 84:8628–8632. [PubMed: 3317417]
3. Westermark P, Andersson A, Westermark GT. Islet Amyloid Polypeptide, Islet Amyloid, and Diabetes Mellitus. Physiol Rev. 2011; 91:795–826. [PubMed: 21742788]
4. Montane J, Klimek-Abercrombie A, Potter KJ, Westwell-Roper C, Bruce Verchere C. Metabolic stress, IAPP and Islet Amyloid. Diabetes, Obes. Metab. 2012; (14 Suppl 3):68–77. [PubMed: 22928566]
5. Cao P, Marek P, Noor H, Patsalo V, Tu L-H, Wang H, Abedini A, Raleigh DP. Islet Amyloid: From Fundamental Biophysics to Mechanisms of Cytotoxicity. FEBS Lett. 2013; 587:1106–1118. [PubMed: 23380070]

6. Cao P, Raleigh DP. Folding and Aggregation of Islet Amyloid Polypeptide: from Physical Chemistry to Cell Biology. Curr. Opinion Struct. Biol. 2013; 23:82–88.
7. Abedini A, Schmidt AM. Mechanisms of Islet Amyloidosis Toxicity in Type 2 Diabetes. FEBS Lett. 2013; 587:1119–1127. [PubMed: 23337872]
8. Westermark GT, Westermark P, Berne C, Korsgren O, Transpla NNCI. Widespread Amyloid Deposition in Transplanted Human Pancreatic Islets. N. Engl. J. Med. 2008; 359:977–979. [PubMed: 18753660]
9. Potter KJ, Abedini A, Marek P, Klimek AM, Butterworth S, Driscoll M, Baker R, Nilsson MR, Warnock GL, Oberholzer J, Bertera S, Trucco M, Korbutt GS, Fraser PE, Raleigh DP, Verchere CB. Islet Amyloid Deposition Limits the Viability of Human Islet Grafts But Not Porcine Islet Grafts. PNAS. 2010; 107:4305–4310. [PubMed: 20160085]
10. Martinez-Alvarez RM, Volkoff H, Cueto JAM, Delgado MJ. Molecular Characterization of Calcitonin Gene-Related Peptide (CGRP) Related Peptides (CGRP, Amylin, Adrenomedullin and Adrenomedullin-2/Intermedin) in Goldfish (Carassius auratus): Cloning and Distribution. Peptides. 2008; 29:1534–1543. [PubMed: 18539360]
11. Westermark GT, Falkmer S, Steiner DF, Chan SJ, Engstrom U, Westermark P. Islet Amyloid Polypeptide is Expressed in the Pancreatic Islet Parenchyma of the Teleostean Fish, Myoxocephalus (cottus) scorpius. Comp. Biochem. Physiol. Part B: Biochem. Mol. Biol. 2002; 133:119–125.
12. Fortin JS, Santamaria-Bouvier A, Lair S, Dallaire AD, Benoit-Biancamano MO. Anatomic and Molecular Characterization of the Endocrine Pancreas of a Teleostean Fish: Atlantic Wolffish (Anarhichas lupus). Zool. Stud. 2015:54.
13. Falkmer S. Experimental Diabetes Research in Fish. Acta Endocrinol. Suppl (Copenh). 1961; 37(Suppl 59):1–122. [PubMed: 13698046]
14. Nguyen TM, Wright JR Jr, Nielsen PF, Conlon JM. Characterization of the Pancreatic Hormones from the Brockmann Body of the Tilapia: Implications for Islet Xenograft Studies. Comp. Biochem. Physiol. Part C: Pharmacol., Toxicol. Endocrinol. 1995; 111:33–44.
15. Yang H, Dickson BC, O'Hali W, Kearns H, Wright JR Jr. Functional Comparison of Mouse, Rat, and Fish Islet Grafts Transplanted into Diabetic Nude Mice. Gen. Comp. Endocrinol. 1997; 106:384–388. [PubMed: 9204372]
16. Hobbs JR, Morgan AD. Fluorescence Microscopy with Thioflavine-T in Diagnosis of Amyloid. J. Pathol. Bacteriol. 1963; 86:437–442. [PubMed: 14068952]
17. Levine H. Thioflavine-T Interaction with Synthetic Alzheimers-Disease Beta-Amyloid Peptides - Detection of Amyloid Aggregation in Solution. Protein Sci. 1993; 2:404–410. [PubMed: 8453378]
18. Sulatskaya AI, Maskevich AA, Kuznetsova IM, Uversky VN, Turoverov KK. Fluorescence Quantum Yield of Thioflavin T in Rigid Isotropic Solution and Incorporated into the Amyloid Fibrils. PLoS One. 2010; 5:e15385. [PubMed: 21048945]
19. Wu C, Wang ZX, Lei HX, Duan Y, Bowers MT, Shea J-E. The Binding of Thioflavin T and Its Neutral Analog BTA-1 to Protofibrils of the Alzheimer's Disease Aβ16–22 Peptide Probed by Molecular Dynamics Simulations. J. Mol. Biol. 2008; 384:718–729. [PubMed: 18851978]
20. Wu C, Biancalana M, Koide S, Shea J-E. Binding Modes of Thioflavin-T to the Single-Layer beta-Sheet of the Peptide Self-Assembly Mimics. J. Mol. Biol. 2009; 394:627–633. [PubMed: 19799914]
21. Wu C, Bowers MT, Shea J-E. On the Origin of the Stronger Binding of PIB over Thioflavin T to Protofibrils of the Alzheimer Amyloid-beta Peptide: A Molecular Dynamics Study. Biophys. J. 2011; 100:1316–1324. [PubMed: 21354405]
22. Cloe AL, Orgel JPRO, Sachleben JR, Tycko R, Meredith SC. The Japanese Mutant Abeta (DeltaE22-Abeta(1–39)) Forms Fibrils Instantaneously, with Low-Thioflavin T Fluorescence: Seeding of Wild-Type Abeta(1–40) into Atypical Fibrils by DeltaE22-Abeta(1–39). Biochemistry. 2011; 50:2026–2039. [PubMed: 21291268]
23. Marek P, Woys AM, Sutton K, Zanni MT, Raleigh DP. Efficient Microwave-Assisted Synthesis of Human Islet Amyloid Polypeptide Designed to Facilitate the Specific Incorporation of Labeled Amino Acids. Organic letters. 2010; 12:4848–4851. [PubMed: 20931985]

24. Abedini A, Raleigh DP. Incorporation of Pseudoproline Derivatives Allows the Facile Synthesis of Human IAPP, a Highly Amyloidogenic and Aggregation-Prone Polypeptide. Org. Lett. 2005; 7:693–696. [PubMed: 15704927]
25. Duan Y, Chowdhury S, Xiong G, Wu C, Zhang W, Lee T, Cieplak P, Caldwell J, Luo R, Wang J, Kollman PA. A Point-Charge Force Field for Molecular Mechanics Simulations of Proteins Based on Condensed-Phase QM Calculations. J. Comput. Chem. 2003; 24:1999–2012. [PubMed: 14531054]
26. Gessel MM, Wu C, Li H, Bitan G, Shea J-E, Bowers MT. Aβ(39–42) Modulates Aβ Oligomerization But Not Fibril Formation. Biochemistry. 2011; 51:108–117. [PubMed: 22129303]
27. Wu C, Bowers MT, Shea JE. Molecular Structures of Quiescently Grown and Brain-Derived Polymorphic Fibrils of the Alzheimer Amyloid $A\beta_{9-40}$ Peptide: A Comparison to Agitated Fibrils. PLoS Comput. Biol. 2010:6.
28. Wu C, Wang ZX, Lei HX, Zhang W, Duan Y. Dual Binding Modes of Congo Red to Amyloid Protofibril Surface Observed in Molecular Dynamics Simulations. J. Am. Chem. Soc. 2007; 129:1225–1232. [PubMed: 17263405]
29. Jorgensen WL, Chandrasekhar J, Madura JD, Impey RW, Klein ML. Comparisons of Simple Potential Functions for Simulating Liquid Water. J. Chem. Phys. 1983; 79:926–935.
30. Wang JM, Wolf RM, Caldwell JW, Kollman PA, Case DA. Development and Testing of a General Amber Force Field. J. Comput. Chem. 2004; 25:1157–1174. [PubMed: 15116359]
31. Essmann U, Perera L, Berkowitz ML, Darden TA, Lee H, Pedersen LG. A Smooth Particle Mesh Ewald Method. J. Chem. Phys. 1995; 103:8577–8593.
32. Ryckaert J-P, Ciccotti G, Berendsen HJC. Numerical Integration of the Cartesian Equations of Motion of a System with Constraints: Molecular Dynamics of n-Alkanes. J. Comput. Phys. 1977; 23:327–341.
33. Procacci P, Berne BJ. Multiple Time-Scale Methods for Constant-Pressure Molecular-Dynamics Simulations of Molecular-Systems. Mol. Phys. 1994; 83:255–272.
34. Chiu SW, Clark M, Subramaniam S, Jakobsson E. CollectiveMotion Artifacts Arising in Long-Duration Molecular Dynamics Simulations. J. Comput. Chem. 2000; 21:121–131.
35. Harvey SC, Tan RKZ, Cheatham TE. The Flying Ice Cube: Velocity Rescaling in Molecular Dynamics Leads to Violation of Energy Equipartition. J. Comput. Chem. 1998; 19:726–740.
36. Wiltzius JJW, Sievers SA, Sawaya MR, Cascio D, Popov D, Riekel C, Eisenberg D. Atomic Structure of the Cross-Beta Spine of Islet Amyloid Polypeptide (Amylin). Protein Sci. 2008; 17:1467–1474. [PubMed: 18556473]
37. Luca S, Yau WM, Leapman R, Tycko R. Peptide Conformation and Supramolecular Organization in Amylin Fibrils: Constraints from Solid-State NMR. Biochemistry. 2007; 46:13505–13522. [PubMed: 17979302]
38. Bedrood S, Li Y, Isas JM, Hegde BG, Baxa U, Haworth IS, Langen R. Fibril Structure of Human Islet Amyloid Polypeptide. J. Biol. Chem. 2012; 287:5235–5241. [PubMed: 22187437]
39. Westermark P, Engstrom U, Johnson KH, Westermark GT, Betsholtz C. Islet Amyloid Polypeptide Pinpointing Amino Acid Residues Linked to Amyloid Fibril Formation. PNAS. 1990; 87:5036–5040. [PubMed: 2195544]
40. Ashburn TT, Lansbury PT. Interspecies Sequence Variations Affect the Kinetics and Thermodynamics of Amyloid Formation - Peptide Models of Pancreatic Amyloid. J. Am. Chem. Soc. 1993; 115:11012–11013.
41. Betsholtz C, Christmansson L, Engstrom U, Rorsman F, Svensson V, Johnson KH, Westermark P. Sequence Divergence in a Specific Region of Islet Amyloid Polypeptide (IAPP) Explains Differences in Islet Amyloid Formation between Species. FEBS Lett. 1989; 251:261–264. [PubMed: 2666169]
42. Buchanan LE, Dunkelberger EB, Tran HQ, Cheng P-N, Chiu C-C, Cao P, Raleigh DP, de Pablo JJ, Nowick JS, Zanni MT. Mechanism of IAPP Amyloid Fibril Formation Involves an Intermediate with a Transient Beta-Sheet. PNAS. 2013; 110:19285–19290. [PubMed: 24218609]
43. Green J, Goldsbury C, Min T, Sunderji S, Frey P, Kistler J, Cooper G, Aebi U. Full-Length Rat Amylin Forms Fibrils Following Substitution of Single Residues from Human Amylin. J. Mol. Biol. 2003; 326:1147–1156. [PubMed: 12589759]

44. Jha S, Snell JM, Sheftic SR, Patil SM, Daniels SB, Kolling FW, Alexandrescu AT. pH Dependence of Amylin Fibrillization. Biochemistry. 2014; 53:300–310. [PubMed: 24377660]
45. Thompson MJ, Sievers SA, Karanicolas J, Ivanova MI, Baker D, Eisenberg D. The 3D Profile Method for Identifying Fibril-Forming Segments of Proteins. PNAS. 2006; 103:4074–4078. [PubMed: 16537487]
46. Chakraborty S, Chatterjee B, Basu S. A Mechanistic Insight into the Amyloidogenic Structure of hIAPP Peptide Revealed from Sequence Analysis and Molecular Dynamics Simulation. Biophys. Chem. 2012; 168:1–9. [PubMed: 22750265]
47. Hamodrakas SJ, Liappa C, Iconomidou VA. Consensus Prediction of Amyloidogenic Determinants in Amyloid Fibril-Forming Proteins. Int. J. Biol. Macromol. 2007; 41:295–300. [PubMed: 17477968]
48. Tartaglia GG, Vendruscolo M. The Zyggregator Method for Predicting Protein Aggregation Propensities. Chem. Soc. Rev. 2008; 37:1395–1401. [PubMed: 18568165]
49. Trovato A, Seno F, Tosatto SCE. The PASTA Server for Protein Aggregation Prediction. Protein Eng., Des. Sel. 2007; 20:521–523. [PubMed: 17720750]
50. Fernandez-Escamilla A-M, Rousseau F, Schymkowitz J, Serrano L. Prediction of Sequence-Dependent and Mutational Effects on the Aggregation of Peptides and Proteins. Nat. Biotechnol. 2004; 22:1302–1306. [PubMed: 15361882]
51. Roland BP, Kodali R, Mishra R, Wetzel R. A Serendipitous Survey of Prediction Algorithms for Amyloidogenicity. Biopolymers. 2013; 100:780–789. [PubMed: 23893755]
52. Tu L-H, Raleigh DP. Role of Aromatic Interactions in Amyloid Formation by Islet Amyloid Polypeptide. Biochemistry. 2013; 52:333–342. [PubMed: 23256729]
53. Moran SD, Zanni MT. How to Get Insight into Amyloid Structure and Formation from Infrared Spectroscopy. J. Phys. Chem. Lett. 2014; 5:1984–1993. [PubMed: 24932380]
54. Reddy AS, Wang L, Singh S, Ling YL, Buchanan L, Zanni MT, Skinner JL, de Pablo JJ. Stable and Metastable States of Human Amylin in Solution. Biophys. J. 2010; 99:2208–2216. [PubMed: 20923655]
55. Marek PJ, Patsalo V, Green DF, Raleigh DP. Ionic Strength Effects on Amyloid Formation by Amylin Are a Complicated Interplay among Debye Screening, Ion Selectivity, and Hofmeister Effects. Biochemistry. 2012; 51:8478–8490. [PubMed: 23016872]
56. Kodali R, Williams AD, Chemuru S, Wetzel R. A beta(1–40) Forms Five Distinct Amyloid Structures Whose Beta-Sheet Contents and Fibril Stabilities Are Correlated. J. Mol. Biol. 2010; 401:503–517. [PubMed: 20600131]
57. Lindberg DJ, Wranne MS, Gatty MG, Westerlund F, Esbjorner EK. Steady-State and Time-Resolved Thioflavin-T Fluorescence Can Report on Morphological Differences in Amyloid Fibrils Formed by A Beta(1–40) and A Beta(1–42). Biochem. Biophys. Res. Commun. 2015; 458:418–423. [PubMed: 25660454]
58. Chen S, Berthelier V, Hamilton JB, O'Nuallain B, Wetzel R. Amyloid-like Features of Polyglutamine Aggregates and Their Assembly Kinetics. Biochemistry. 2002; 41:7391–7399. [PubMed: 12044172]
59. O'Brien TD, Westermark P, Johnson KH. Islet Amyloid Polypeptide and Calcitonin Gene-Related Peptide Immunoreactivity in Amyloid and Tumor Cells of Canine Pancreatic Endocrine Tumors. Vet. Pathol. 1990; 27:194–198. [PubMed: 1972303]

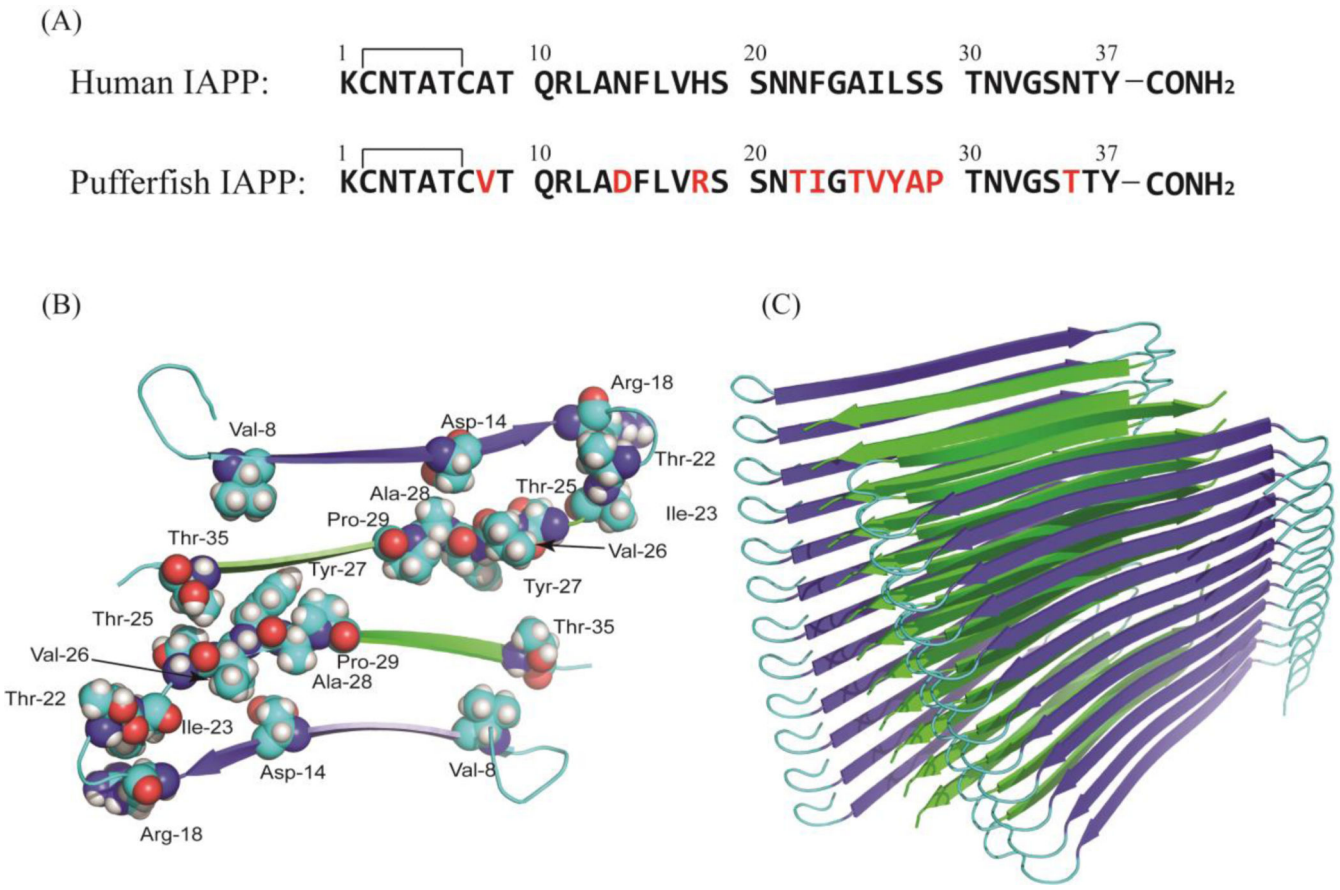

Figure-1.

(A) Comparison of the primary sequence of human IAPP and pufferfish IAPP. Residues which differ from the human peptide are colored red. Both sequences have amidated C-termini and contain a disulfide bond between residues 2 and 7. (B) Cross-section of a model of the human IAPP amyloid fibril based on crystal structures of fragments of the molecule. Residues in pufferfish IAPP which differ from the human sequence are built into the model and are shown in space filling format. (C) Ribbon diagram of the fibril.

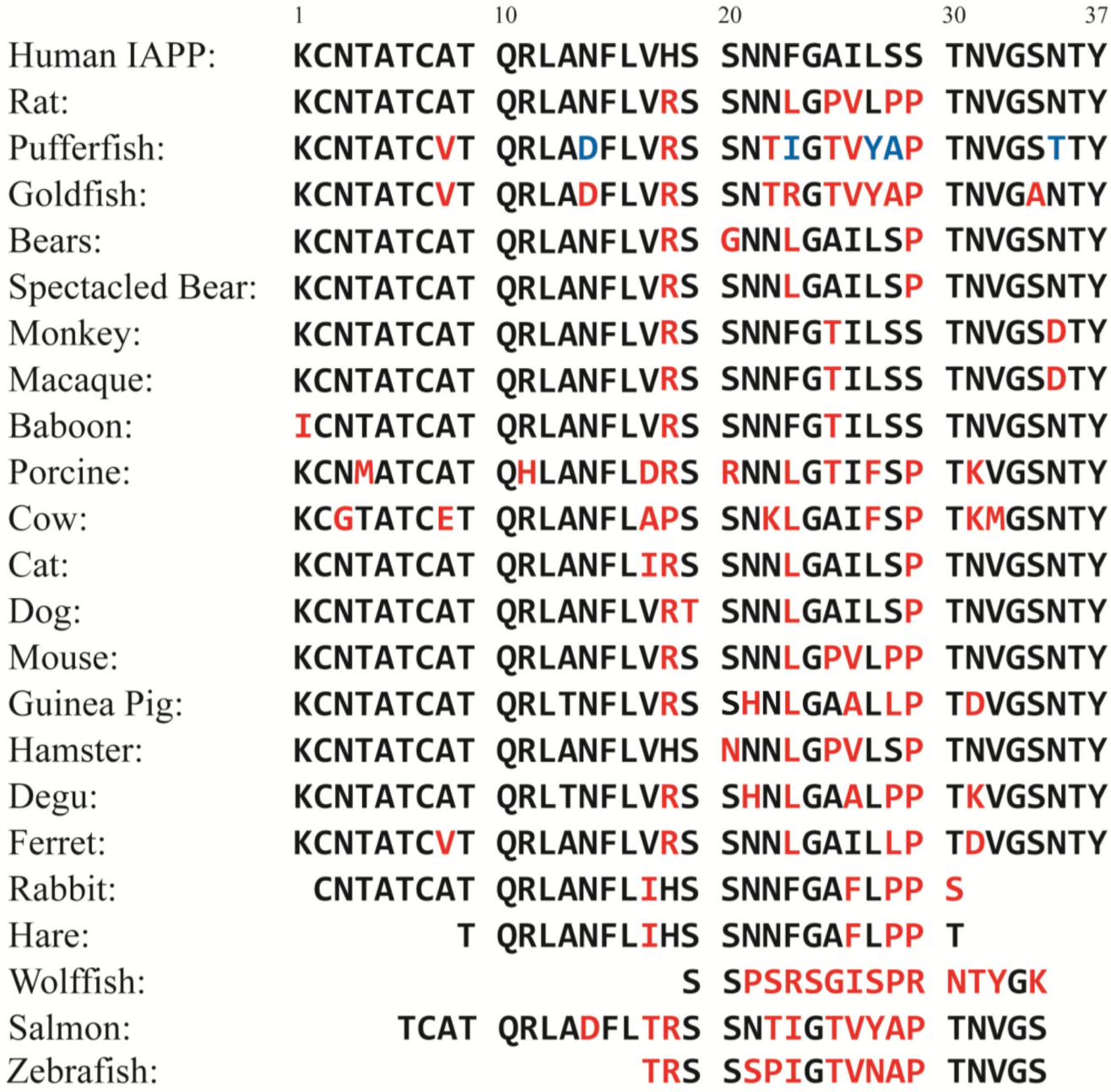

Figure-2.

Primary sequences of IAPP from different species. Residues that differ from the human sequence are colored. Substitutions which are in pufferfish IAPP but not in mammalian IAPP sequences are color coded blue. All of the variants contain a disulfide bridge between Cys-2 and Cys-7 and all have an amidated C-terminus. Primates and cats have been reported to develop diabetes and form islet amyloid, but rodents do not. Dog IAPP does form islet amyloid in canine pancreatic endocrine tumors.[59] Ferret and porcine IAPP are reported to be significantly less amyloidogenic than human IAPP. The ability of baboon, bear, bovine and spectacled bear IAPP to form amyloid *in vitro* has not been investigated. Islet amyloid is

found in the degu, a rodent, but degu islet amyloid is derived from insulin. Only partial sequences are available for rabbit, hare, wolffish, zebrafish and Atlantic salmon IAPP.

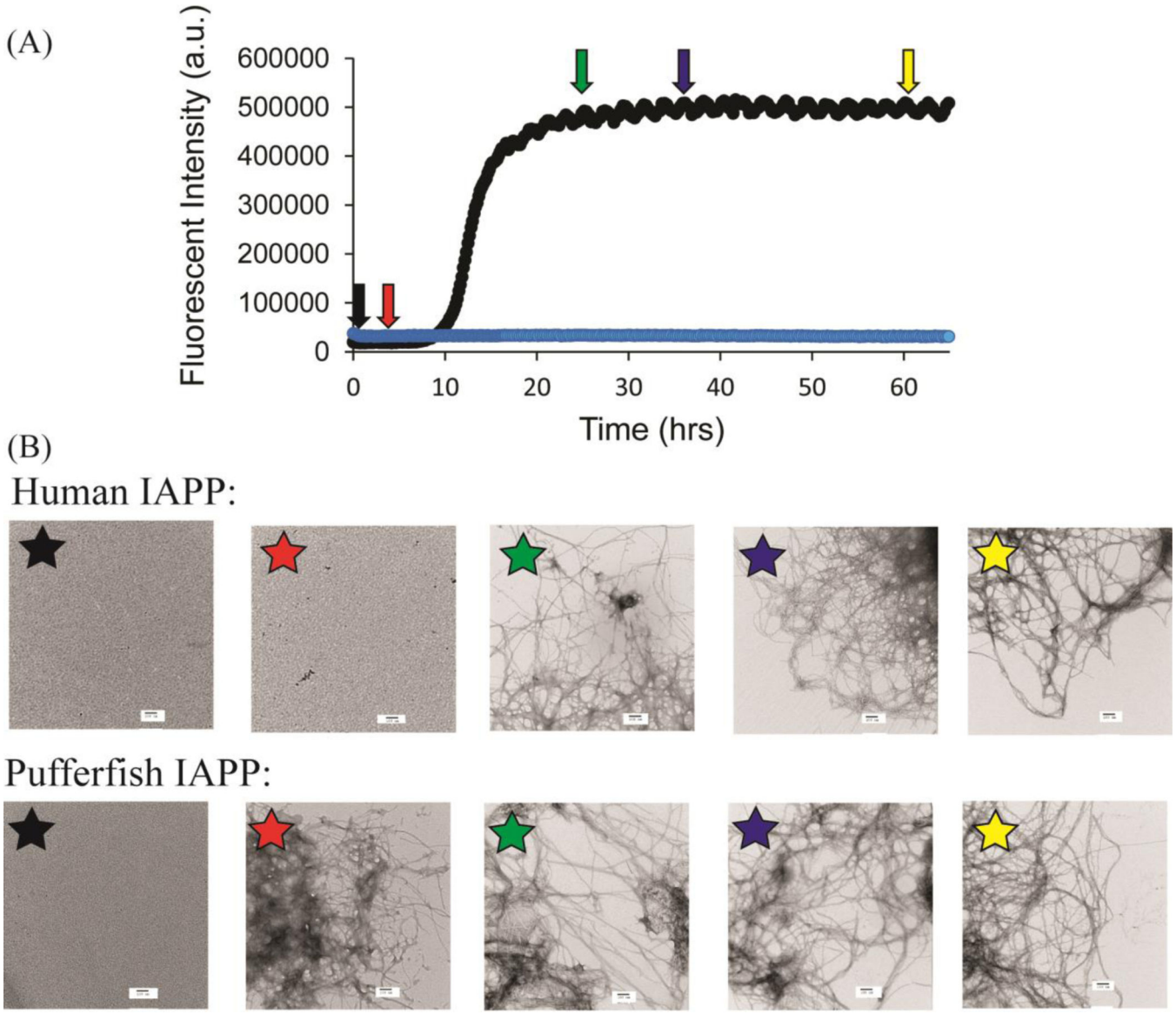

Figure-3.

Analysis of amyloid formation by pufferfish IAPP (blue) and human IAPP (black) in 20 mM tris-HCl at pH 7.4. (A) Fluorescence monitored thioflavin-T assays of amyloid formation. No change in thioflavin-T fluorescence is detected for the pufferfish peptide over the entire time course of the experiment. Arrows indicate times, at which aliquots where collected for TEM analysis. (B) TEM images of samples of human IAPP (top) and pufferfish IAPP (bottom) collected at the different time points. Experiments were conducted with 16 μM IAPP, 32 μM thioflavin-T at 25 °C in 20 mM tris-HCl at pH 7.4. Scale bars in TEM images represent 100 nm.

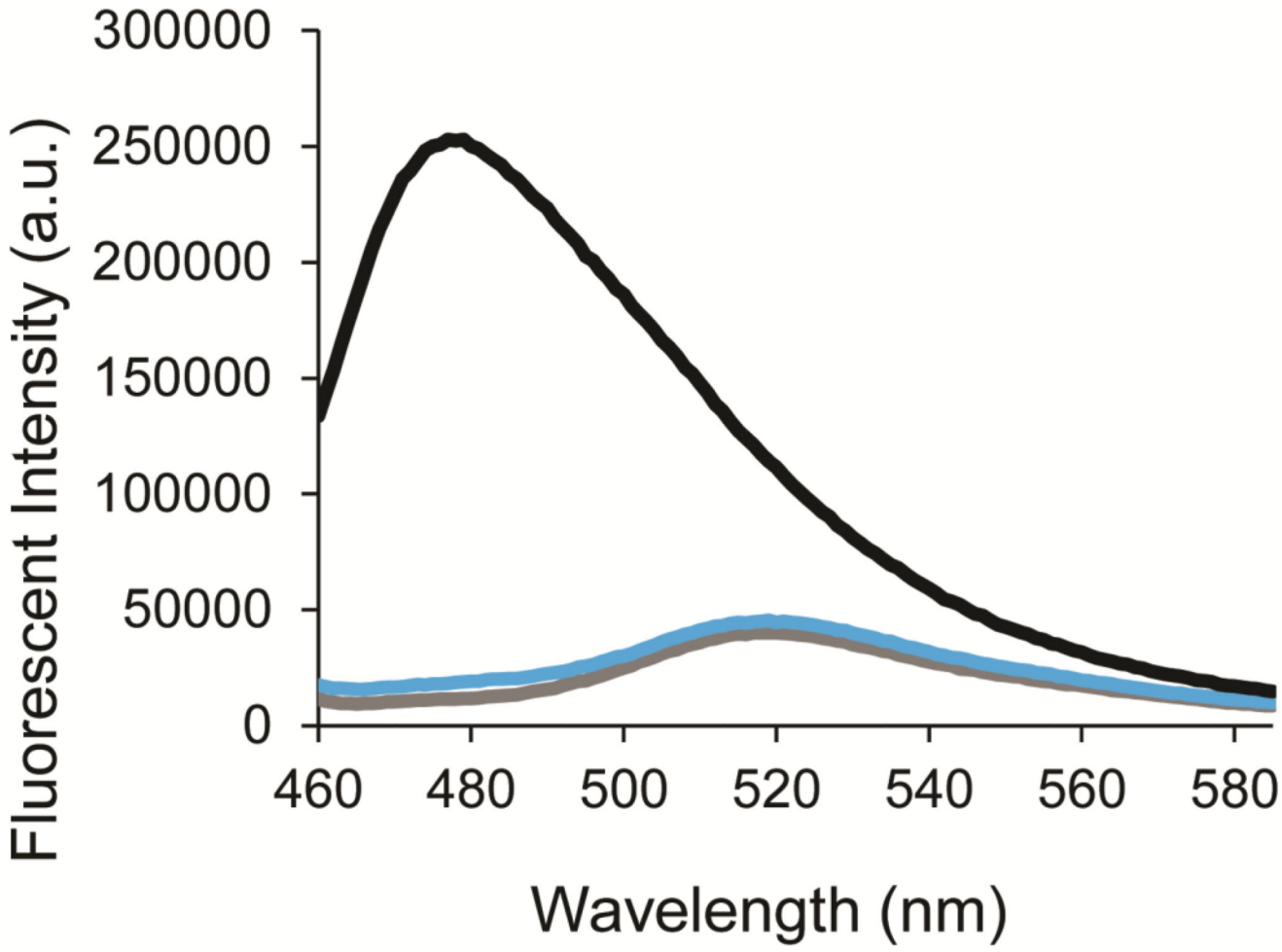

Figure-4.

Thioflavin-T emission spectra of samples of 32 μM thioflavin-T, with human IAPP (black), pufferfish IAPP amyloid fibrils (blue), and thioflavin-T alone (grey). IAPP when present is at 16 μM in monomer concentration. Spectra were recorded at the end of the kinetic experiments depicted in Figure 2. Samples contained 20 mM tris-HCl at pH 7.4 and measurements were made at 25 °C. Excitation at 450 nm.

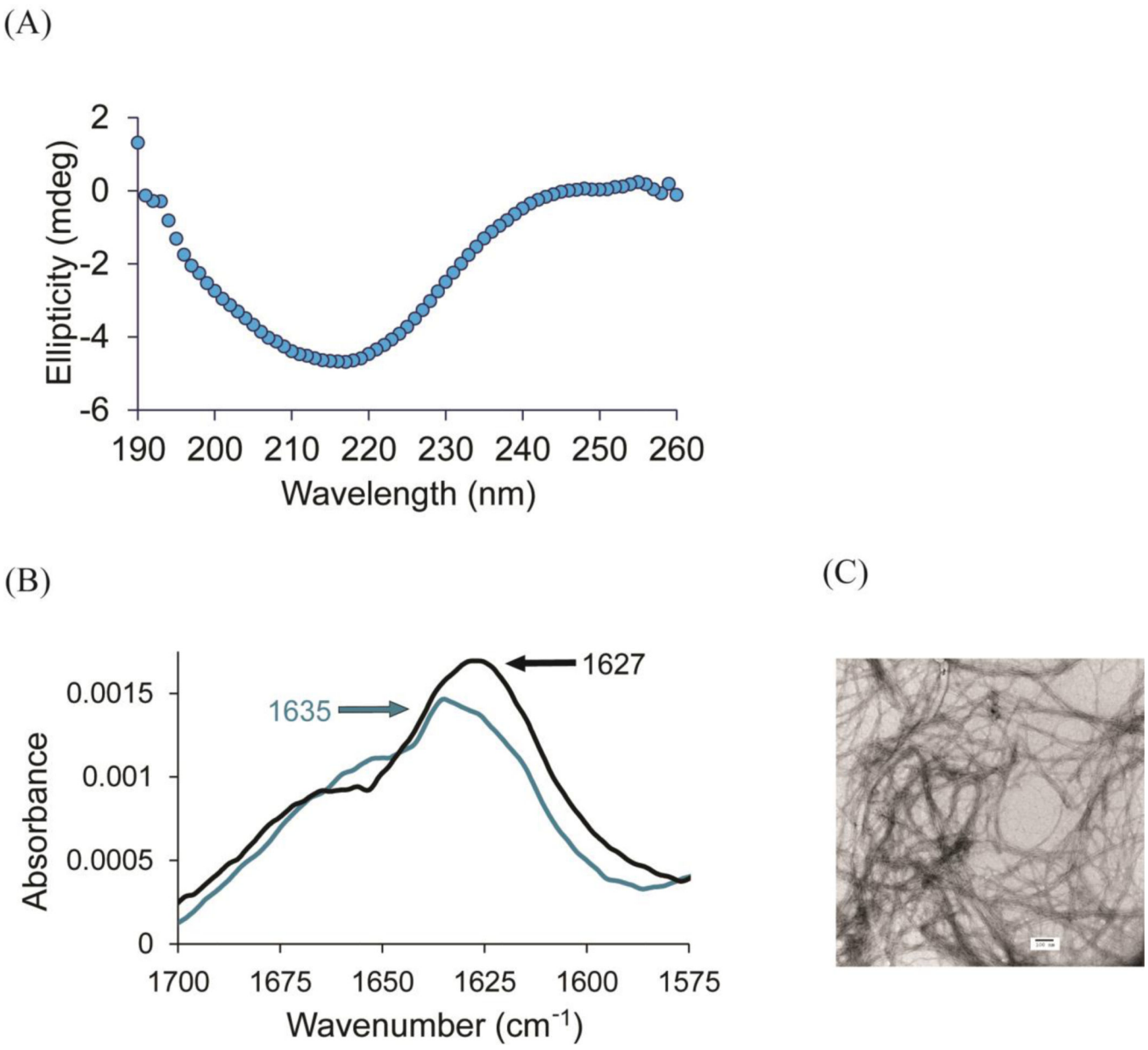

Figure-5.

Pufferfish IAPP forms fibrils with significant β-sheet secondary structure. (A) CD spectrum of a sample of the fibril material formed by a 40 μM sample of pufferfish IAPP. The spectrum is the smoothed average of three scans. (B) FTIR spectra of p-IAPP (blue) and h-IAPP (black). (C) TEM image of the pufferfish IAPP sample collected at time of CD measurement. Samples were incubated at 25 °C. Scale bars in TEM images represent 100 nm.

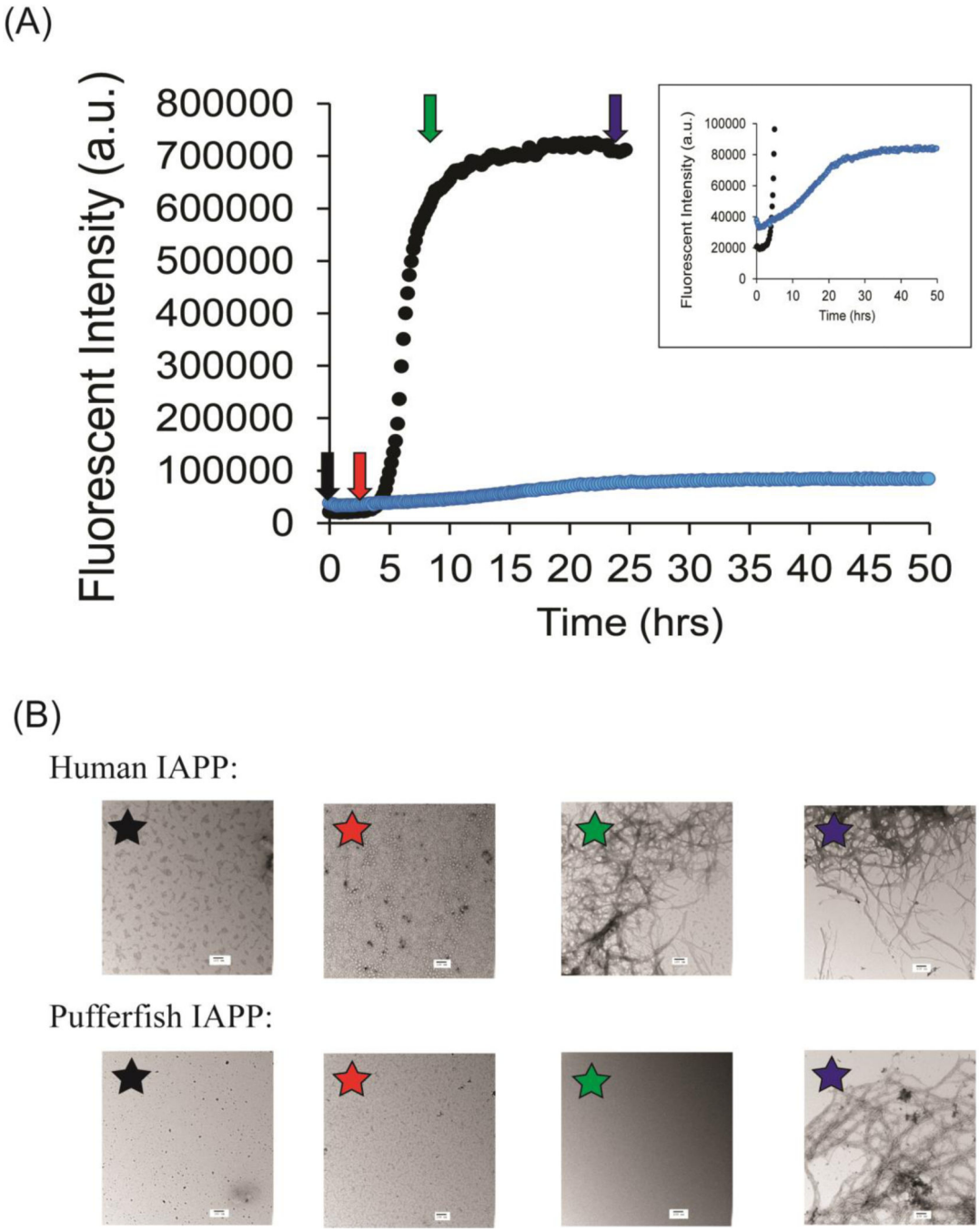

Figure-6.

Analysis of the ability of pufferfish IAPP to form amyloid in phosphate buffered saline solution. (A) Fluorescence monitored thioflavin-T assays of human IAPP (black) and pufferfish IAPP (blue) amyloid formation in 20 mM sodium phosphate, 140 mM potassium chloride at pH 7.4. Arrows indicate times at which aliquots where collected for TEM analysis. Aliquots were collected at t = 0 (black), 3 hrs (red), 7 hrs (green), and 24 hrs (blue) (B) TEM images of samples human IAPP (top) and pufferfish IAPP (bottom) collected at the different time points. Experiments were conducted with 16 μM IAPP, 32 μM thioflavin-T

at 25 °C in 20 mM sodium phosphate, 140 mM potassium chloride at pH 7.4. Scale bars in TEM images represent 100 nm.

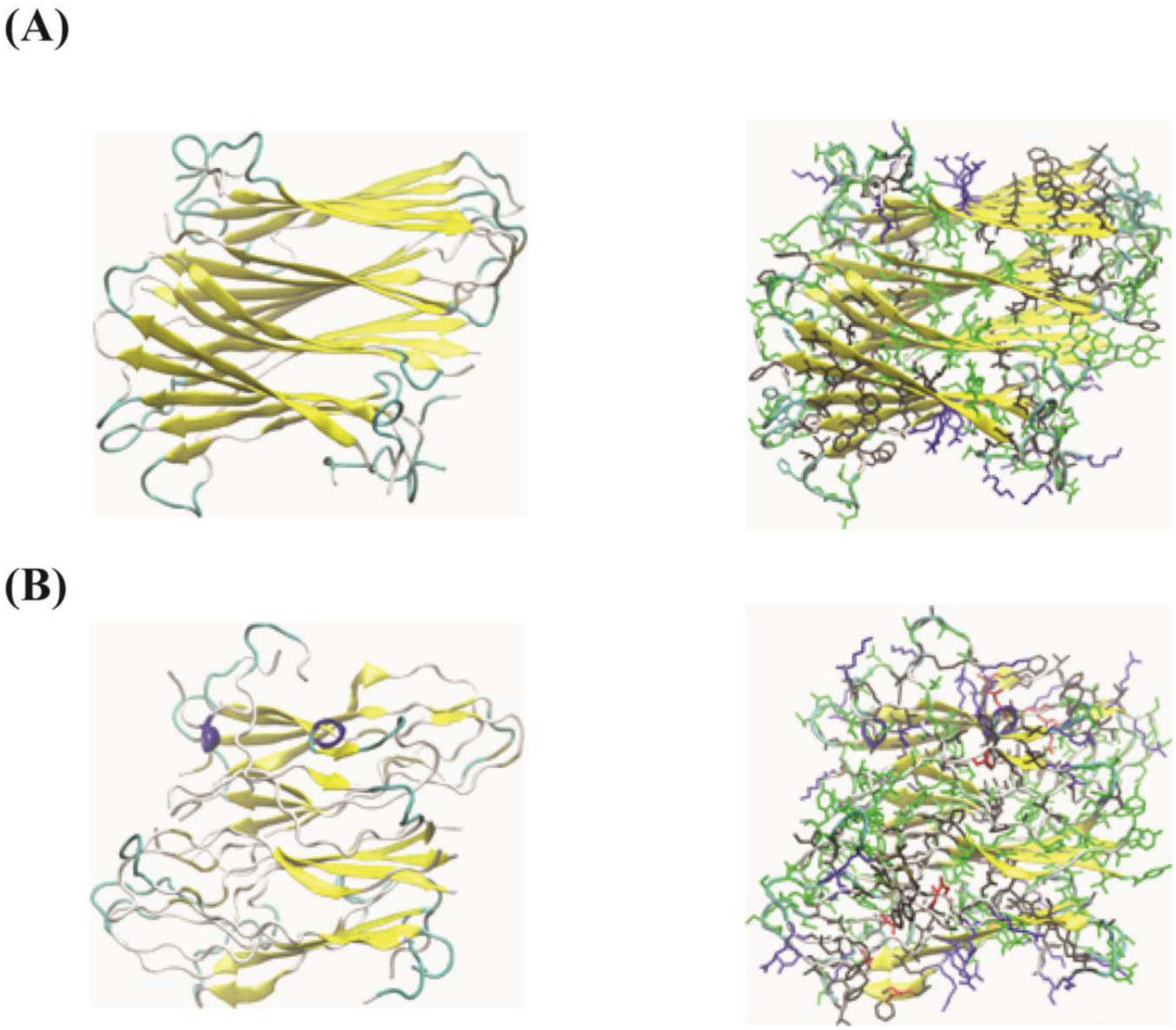

Figure-7.

Last snapshots of two representative simulations. (A) Human IAPP fibril model from the solid state NMR study. (B) Pufferfish IAPP fibril model is derived from the NMR model by threading. 3_{10}, α-helical, β-strand, turn and coiled conformations are colored in blue, yellow, cyan and white respectively. Sidechains are color-coded as; blue, positively charged; red, negatively charged; black, hydrophobic; and green, hydrophilic.

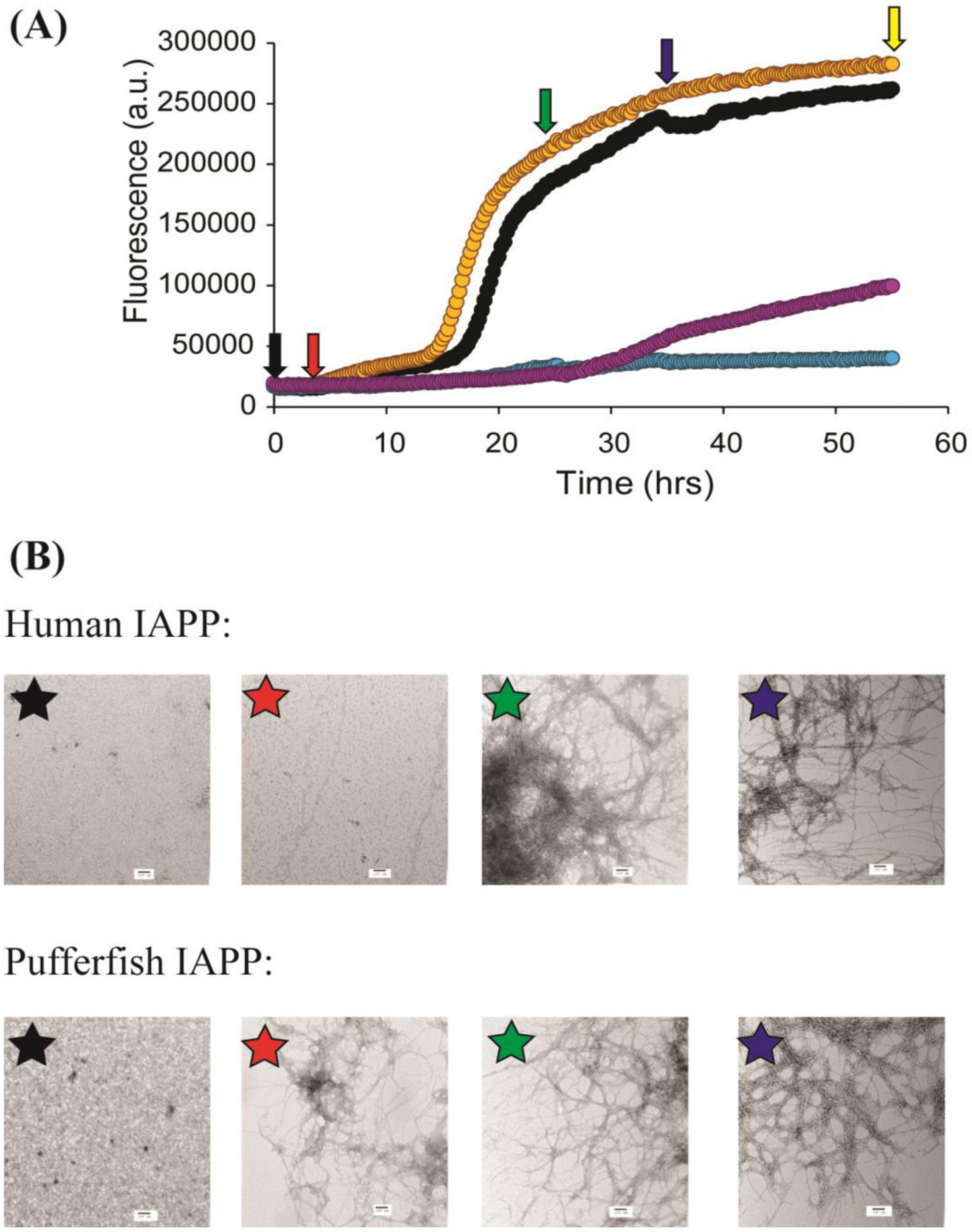

Figure-8.

Analysis of amyloid formation by pufferfish IAPP and human IAPP in the presence of excess thioflavin-T in 20 mM tris-HCl at pH 7.4. (A) Fluorescence monitored thioflavin-T assays of human IAPP with 2-fold and 20-fold excess of thioflavin-T (black and orange respectively) and of pufferfish IAPP with 2-fold and 20-fold excess of the dye (blue and purple respectively). Arrows indicate times at which aliquots were collected for TEM analysis. Aliquots were collected at t = 0 (black), $0.25t_{50}$ (red), $2t_{50}$ (green), $3t_{50}$ (blue), and $5t_{50}$ (yellow), where t_{50} refers to the time required for human IAPP to reach half maximum

fluorescence intensity in a thioflavin-T assay. (B) TEM images of samples of human IAPP (top) and pufferfish IAPP (bottom) in the presence of 20-fold excess of thioflavin-T collected at different time points. Experiments were conducted with 16 μM IAPP, 32 μM or 320 μM thioflavin-T at 25 °C in 20 mM tris-HCl at pH 7.4. Scale bars in TEM images represent 100 nm.